Available online at www.sciencedirect.com
SCIENCE DIRECT®
International Journal of Heat and Mass Transfer 47 (2004) 363–371
International Journal of HEAT and MASS TRANSFER
www.elsevier.com/locate/ijhmt

3D unsteady numerical analysis of conjugate heat transport and turbulent/laminar flows in LEC growth of GaAs crystals

O.V. Smirnova [a,*], V.V. Kalaev [b]

[a] Soft-Impact Ltd., 27 Engels av., P.O. Box 33, 194156 St. Petersburg, Russia
[b] Semiconductor Technology Research GmbH, Erlangen, Germany

Received 30 November 2002; received in revised form 18 March 2003

Abstract

We present the conjugated 3D unsteady numerical analysis of industrial-scale LEC GaAs crystal growth, including the calculation of heat transfer in the crystal and crucibles, melt convection, and the encapsulant flow. The analysis of unsteady turbulent melt convection is performed in terms of the large eddy simulation approach. A special procedure was introduced into the calculations to predict the geometry of the crystallization front. The results of the 3D unsteady calculations are compared to the results obtained in terms of the conventional steady-state Reynolds averaged approach with respect to the calculation of the geometry of the crystallization front. The effect of convective heat transfer in the encapsulant is specially studied using the 3D unsteady analysis. To investigate details of dynamic interaction between two immiscible liquids having a plane interface, preliminary computational tests were performed in a model setup.

1. Introduction

Numerical simulation has become a useful tool for understanding and optimization of physical mechanisms during crystal growth in general and during the liquid encapsulated Czochralski (LEC) growth [1] in particular because an experimental approach is often hardly applicable and sufficiently expensive due to high temperatures and complexity of growth apparatuses. However, a really profitable application of computational results is only possible if the computations provide data with an accuracy required in engineering work. In the case of LEC growth of large GaAs crystals, the geometry of the crystallization front, which should be controlled, is affected by several physical phenomena: first of all, by the regime of radiative heat exchange in the whole growth chamber; second, by heat loss through the growing crystal and heat release due to the crystallization; and third, by conductive and convective heat transfer in the melt, encapsulant, and surrounding inert gas. For the GaAs LEC crystal growth, there are a number of papers describing computations of global radiative and conductive heat transfer [2,3], studying gas convection [2,4–7], simulating melt convection in 2D [2,5,8,9] and 3D [10,11] approximations. A difficulty in simulating the melt flow is the fact that the flow usually has turbulent structure [8–11], which necessitates an application of a specially calibrated turbulence model in the range of the Reynolds averaged Navier–Stokes equations (RANS). An alternative computational way for predicting turbulent flows is the direct numerical simulation (DNS) approach [12] implying all turbulent vertices being directly resolved within a 3D unsteady approximation. As the former approach needs a preliminary calibration of a turbulence model, and DNS requires huge computational resources, we have first applied large eddy simulation (LES) [12] for the calculation of 3D turbulent melt convection of GaAs. Applying LES is much less computer resource consuming than the case of DNS; moreover, results obtained with LES are poorly sensitive to a subgrid scale (SGS) turbulence model simulating

* Corresponding author. Tel.: +7-812-554-45-70; fax: +7-812-326-61-94.
E-mail address: smirnova@softimpact.ru (O.V. Smirnova).

0017-9310/$ - see front matter © 2003 Elsevier Ltd. All rights reserved.
doi:10.1016/S0017-9310(03)00404-6

Nomenclature

C_p	specific heat
g	gravity acceleration
H	crystallization (melting) heat
h	cylinder height
Nu	Nusselt number
p	pressure
Q	heat flux
Ra	Rayleigh number
T	temperature
t	time
V	fluid velocity or the velocity describing rotation of a solid domain
U	buoyancy velocity
u_n	local crystallization rate normal to the crystal surface
x_i	coordinate directions

Greek symbols

β	thermal extension coefficient
ε	emissivity
λ	conductivity
μ	effective viscosity
Θ	time scale
ρ	density
ρ_0	reference density
σ	Stefan–Boltzmann constant
ω	rotation rate

Subscripts

bottom	cylinder bottom
crys	crystal
cruc	crucible
encaps	encapsulant
eff	effective
gas	gas
melt	melt
n	normal component
rad	radiative
top	cylinder top
w	surface
τ	tangent component

Superscript

in	incoming

small turbulence, when large energetic flow structures are directly resolved within a 3D computational grid.

For the calculation of the geometry of the melt/crystal interface and for accounting for a feedback of flows on heat transfer near the crystallization front and crucible surface, we have first developed an extended 3D unsteady approach describing heat transport and convection in a domain containing the crystal, melt, encapsulant, and crucibles (see Fig. 1a). To study details of the complicated liquid/liquid interaction between the turbulent melt and the laminar encapsulant flow having an immiscible boundary with the melt, test calculations in a model setup are presented before engineering calculations.

2. Mathematical model

Heat transfer and flows in the GaAs melt and B_2O_3 encapsulant (Fig. 1a) can be described by the heat conservation equation (1) and the Navier–Stokes equations (2) and (3) with the density depending on the temperature T

$$\frac{\partial(\rho c_p T)}{\partial t} + \nabla \cdot (\rho c_p \vec{V} T) = \nabla \cdot (\lambda_{\text{eff}} \nabla T), \tag{1}$$

$$\nabla \cdot (\rho \vec{V}) = 0, \tag{2}$$

$$\frac{\partial(\rho \vec{V})}{\partial t} + (\vec{V} \cdot \nabla)\rho \vec{V} = -\nabla p + \nabla \cdot \underline{\underline{\tau}} + (\rho - \rho_0)\vec{g},$$

$$\tau_{ij} = \mu_{\text{eff}} \left(\frac{\partial V_i}{\partial x_j} + \frac{\partial V_j}{\partial x_i} \right). \tag{3}$$

The effective conductivity and viscosity are calculated as a sum of the molecular and turbulent quantities (using the turbulent Prandtl number of 0.9 for the calculation of the turbulent conductivity). Properties of liquid and solid materials occurring in the calculations are summarized in Table 1. Turbulent characteristics in terms of the LES approach are calculated using the one equation SGS turbulence model taken from [13], and in the case of pure RANS calculations the low Reynolds number k–ε turbulence model of Chien [14] was applied.

Boundary conditions for the 3D calculations were formulated as follows. The rotation rates of the crystal, ω_{cryst}, and the crucible, ω_{cruc}, were imposed for both liquids by defining the velocity along the melt/crystal and melt/crucible interfaces, respectively. Along the melt/encapsulant interface, the tangential and normal components of the velocity should satisfy Eq. (4)

$$\left(\mu_{\text{eff}} \frac{\partial V_\tau}{\partial n} \right)_{\text{melt}} = \left(\mu \frac{\partial V_\tau}{\partial n} \right)_{\text{encaps}},$$

$$(V_n)_{\text{melt}} = (V_n)_{\text{encaps}} = 0. \tag{4}$$

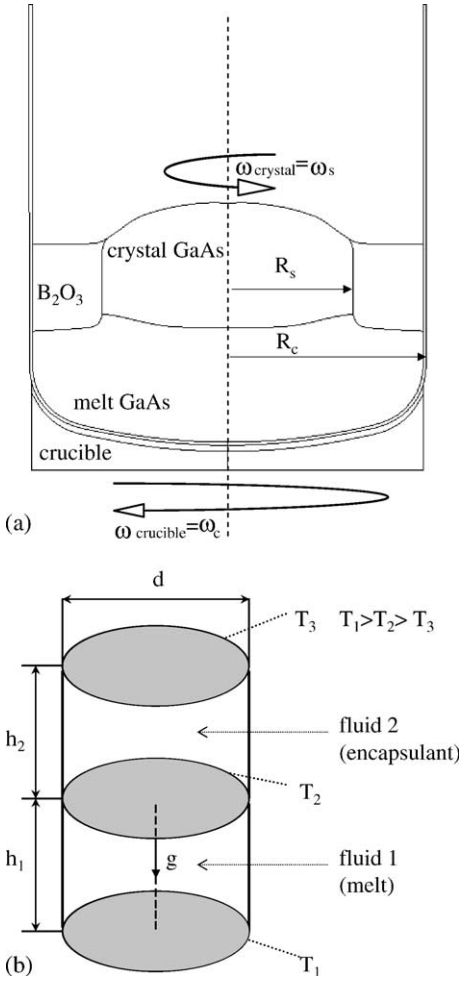

Fig. 1. Schemes of the crystallization zone for GaAs encapsulanted crystal growth (a) and the model setup for modeling interaction of immiscible liquids (b).

The buoyancy is the major driving force for the melt and encapsulant flows; so thermal boundary conditions are of high importance in the calculations. Actually, global heat transfer computations in the whole growth chamber are necessary for the definition of radiative and conductive heat fluxes along an interface inside a growth system. As such global heat transfer analysis is impossible today in a 3D approximation, preliminary computations of heat and mass transfer in the whole growth chamber were performed in a 2D axisymmetric approximation [15,16], and distributions of heat fluxes were extracted for the present 3D analysis. This combined 2D/3D approach is quite reliable for LEC growth because the aim of the 3D calculations is to predict accurately flow characteristics, which is extremely important in the vicinity of the crystallization front and does not practically affect thermal distributions in solid domains disconnected with the near-melt zone under our consideration. The melt–crystal interface temperature is fixed at the crystallization temperature level in the calculations. Using the data obtained by the 2D model of global heat and mass transfer [16], the incoming radiative heat flux $Q_{\mathrm{rad}}^{\mathrm{in}}$ and conductive heat flux Q_{gas} from surrounding gas along external boundaries are preset, and the outgoing radiative heat flux is calculated from the surface temperature T_{w} using the surface emissivity ε, that allows us to formulate the boundary condition for external surfaces of the 3D domain in the following way:

$$\lambda\frac{\partial T}{\partial n} = -Q_{\mathrm{gas}} + \sigma\varepsilon T_{\mathrm{w}}^4 - Q_{\mathrm{rad}}^{\mathrm{in}}. \tag{5}$$

This expression relates the conductive heat flux into the surface to the radiative heat fluxes and conductive gas heat flux; so, the boundary condition is non-linear, reflecting unsteady changes in the temperature due to melt turbulent pulsations. At internal interfaces, the conventional boundary condition imposing a continuous conductive heat flux is used. The crystallization rate u_{n} over the crystallization front of the GaAs crystal can be calculated with the following equation:

$$\rho_{\mathrm{cryst}} H u_{\mathrm{n}} = \left(\lambda\frac{\partial T}{\partial n}\right)_{\mathrm{melt}} - \left(\lambda\frac{\partial T}{\partial n}\right)_{\mathrm{cryst}}. \tag{6}$$

A finite volume method of the 2nd accuracy order in space and in time on block-structured grids, implemented in the CGSim (crystal growth simulator) code developed in our team has been applied to the 3D calculations. A moving grid approach is introduced into the CGSim code to define the geometry of the crystallization front by correcting the grid at the end of each time step. The geometry (for a growth regime) is found if the time-averaged crystallization rate is constant over the interface and equal to a required value.

3. Calculations in a model setup

Before starting numerical analysis for such complicated 3D conjugated problem with turbulent and laminar flows coupled to heat transfer in surrounding solid domains, we performed testing computations in a model setup shown in Fig. 1b. The model setup consists of two cylinders containing fluids having a plane interface and different properties (similar to the melt coexisting with the encapsulant). A particular cylindrical geometry with the diameter equal to the cylinder height was chosen for each fluid because of available experimental [17,18] and computational [19] data suitable for comparing in the case of a single fluid flow with turbulent characteristics. Natural convection in a cylinder could be characterized by the Rayleigh number defined as $Ra = \frac{\beta\rho g(T_{\mathrm{bottom}} - T_{\mathrm{top}})h^3}{\mu\lambda}$. The sidewalls are adiabatic. The intensity of convective

Table 1
Material properties

Density (kg/m³)	
Melt GaAs	$7.33 \times 10^3 - 1.07 \cdot T$
Crystal GaAs	$5.32 \times 10^3 - 9.91 \times 10^{-2} \cdot T$
Felt	2.0×10^2
Graphite EK98	1.75×10^3
Crucible pBN	2.15×10^3
Encapsulant B_2O_3	$2.34 \times 10^3 - 1.5 \cdot T + 9.38 \times 10^{-4} \cdot T^2 - 2.06 \times 10^{-7} \cdot T^3$
Conductivity (W/m K)	
Melt GaAs	1.78×10^1
Crystal GaAs	7.12
Felt	$4.3 \times 10^{-2} + 3.24 \times 10^{-5} \cdot T + 9.4 \times 10^{-8} \cdot T^2$
Graphite EK98	$1.15 \times 10^2 - 9.81 \times 10^{-2} \cdot T + 3.61 \times 10^{-5} \cdot T^2 - 4.29 \times 10^{-9} \cdot T^3$
Crucible pBN	3.25×10^1
Encapsulant B_2O_3	$2.37 \times 10^{-1} + 1.1 \times 10^{-3} \cdot T$
Specific heat (J/kg K)	
Melt GaAs	4.34×10^2
Crystal GaAs	4.24×10^2
Felt	2.00×10^3
Graphite EK98	1.00×10^3
Crucible pBN	2.46×10^3
Encapsulant B_2O_3	1.83×10^3
Dynamic viscosity (kg/m s)	
Melt GaAs	2.79×10^{-3}
Encapsulant B_2O_3	3.73

heat transport can be estimated with the Nusselt number, which can be calculated over a horizontal wall as $Nu = \frac{(\partial T/\partial n)_{\text{wall}}}{(T_{\text{bottom}} - T_{\text{top}})/h}$. For comparing flows having different Rayleigh numbers, it is convenient to introduce a time scale $\Theta = \frac{\pi h}{U}$, here $U = (g\beta(T_{\text{bottom}} - T_{\text{top}})h)^{1/2}$ is the buoyancy velocity. Our computations have been done for $Ra = 2.5 \times 10^4$, $Ra = 10^6$, $Ra = 10^7$, which correspond to laminar and turbulent regimes. The Prandtl number was taken to be 0.022 as in the case of mercury convection. For turbulent regimes, the time periods of approximately 100Θ with a time step of 0.1Θ were calculated after passing a sufficient period transient from an initial flow field. For the case of a single flow (solid upper cylinder or the no-slip boundary condition over the interface between two fluids), the computational results are in good agreement with experiments [18] and data obtained using DNS [19], as it is shown in Fig. 2 for the dependence of the time-averaged Nusselt number on the Rayleigh number. So, the developed computational tool predicts well characteristics of 3D unsteady laminar and turbulent natural convection, which proves its validity for further engineering computations.

Additional calculations in the model setup were performed to study the effect of the encapsulant (the upper fluid) on turbulent characteristics of the melt (the lower fluid). The first calculation was done to simulate crystal growth from the melt without encapsulant (the free surface condition for the upper surface of the lower cylinder). And the second computation was performed with a liquid in the upper cylinder, which is more viscous than the lower liquid as in the case of the melt/encapsulant interaction. The Rayleigh number of 3×10^3 characterizes the upper liquid, and the lower fluid has the Rayleigh number of 10^6 for both cases. To have the

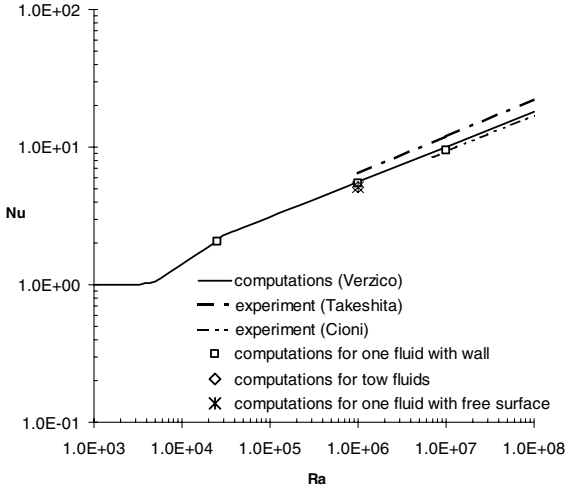

Fig. 2. Dependence of the time-averaged Nusselt number on the Rayleigh number for the model setup.

opportunity in detailed comparison, the Prandtl number for both liquids was the same as in the previous parametric computations.

Fig. 3 shows an instantaneous velocity distribution in the central vertical cross section of the double cylinder for the case of two different fluids. For the upper viscous liquid, the velocity is very low; so the flow field is indicated by stream traces. There are convection structures in the upper and lower fluids, the lower liquid motion is fully turbulent, and convection of the upper liquid is laminar. It is clear, that the motions of the upper and lower liquids are correlated, so the upper fluid flow direction allows us to reveal an averaged direction of the low frequency motion of the lower fluid, which is of high interest for understanding of turbulent natural convection characteristics.

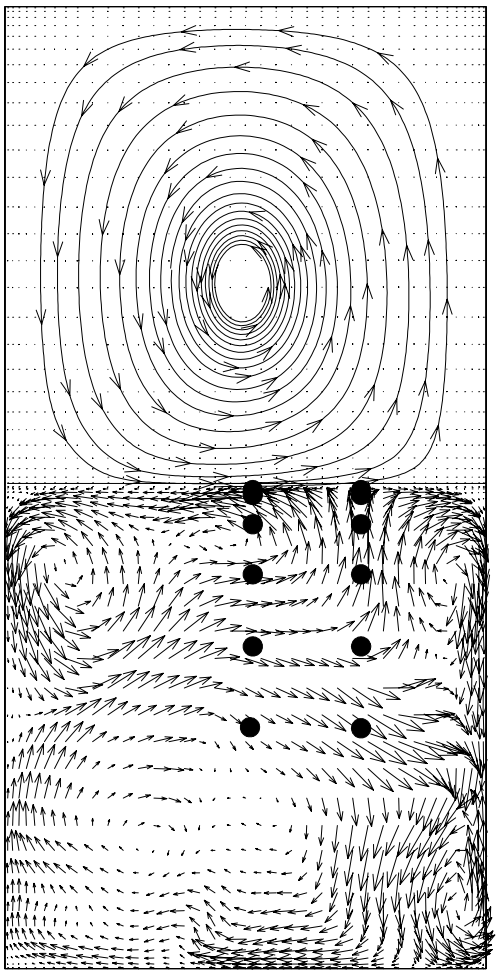

Fig. 3. Instantaneous velocity distribution in the central vertical cross section of the double cylinder with two fluids.

Two rows of monitoring points have been situated in the lower cylinder (see Fig. 3) to obtain detailed information about the turbulent flow for different boundary conditions. The first point group is situated at the centerline, and the second one is at a half radius distance. Instant values of the temperature and velocities were saved for each monitoring point during the whole computational time period. Obtained variation of the turbulent kinetic energy of directly resolved turbulent velocity fluctuations as a function of the distance from the cylinder bottom is presented in Fig. 4. The turbulent kinetic energy in the lower fluid covered by the other fluid, as for variant with a solid wall, vanishes abruptly near the surface, while the turbulent kinetic energy for

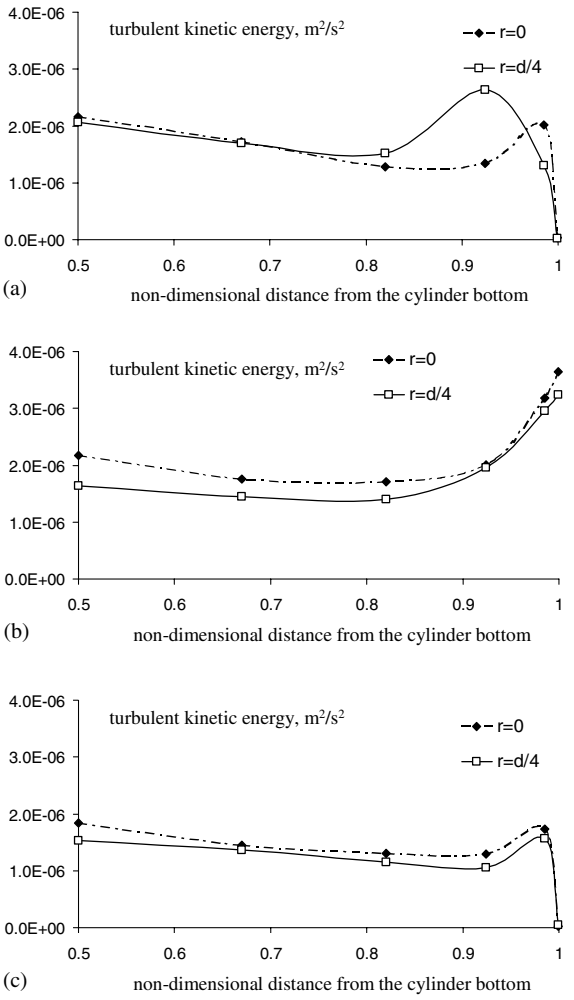

Fig. 4. Variation of the turbulent kinetic energy of resolved velocity fluctuations as a function of the distance form the cylinder bottom for the fluid covered by other fluid (a), for the fluid with the free surface (b), and for the fluid with a solid wall (c).

the fluid with the free surface increases near the boundary. However, the time-averaged Nusselt numbers obtained in the computations for the two fluids, for the fluid limited by a solid wall and for the fluid with the free surface are close to each other (see Fig. 2).

Considering the distributions of the turbulent kinetic energy, one can conclude, that the presence of the upper viscous laminar fluid acts at turbulence characteristics similar to the case with the solid wall. So, it is appropriate to set the turbulent kinetic energy equal zero in turbulence calculations at an interface between two liquids with similar dimensionless parameters.

4. Crystal growth computations

As it has been described above, the 3D calculations of GaAs encapsulated Czochralski crystal growth were carried out in a domain containing the melt, the crystal, the encapsulant, and the crucibles. Heat transfer in solid blocks, 3D unsteady turbulent melt convection, and the laminar encapsulant flow are conjugated in the calculations. The 3D computational grid approximately consisting of 120 000 cells is presented in Fig. 5. The geometry of the near-melt zone under our analysis was taken from the paper [2] together with details about growth conditions. The crystal diameter is 3 in. In the calculations, the crucible rotation is 5 rpm, the crystal rotation is (−5) rpm, and the crystallization rate is 12 mm/h. The Reynolds numbers for the melt flow and for the encapsulant are 6×10^6 and 1.8×10^3, respectively, which is in the range of testing calculations presented in the previous section. The grid is sufficient to resolve largest turbulent vortices, when unresolved directly turbulent structures are simulated using the SGS turbulence model. Instantaneous distributions of the temperature and velocity in the melt and encapsulant are shown in Fig. 6 in a vertical cross section. It is evident that the temperature distribution under the crystal is not axisymmetric, which indicates a complicated heat exchange near the crystallization front. Under the crystal, there is a profound downward melt jet fluctuating at the axis of rotation, with generating spoke turbulent structures round about. In the melt periphery, there are two stable toroidal vortices weakly fluctuating in their size and intensity. The rotation and the buoyancy drive these two vertices to a large extent. Slow encapsulant motion towards the crystal along the melt/encapsulant interface results from the surface tension produced by the melt. However, the buoyancy force mainly affects the toroidal vortex in the upper part of the encapsulant. Although the encapsulant motion is much slower than the melt flow, the contribution of convective heat exchange in the encapsulant is not negligible as it could be seen from the temperature distribution. This is mainly due to a sufficiently low heat conductivity or, in other words, due to

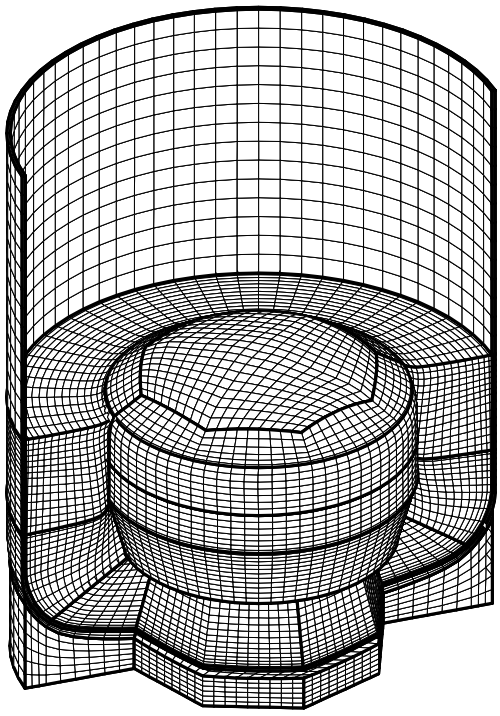

Fig. 5. The 3D computational grid of the near-melt zone in GaAs LEC growth.

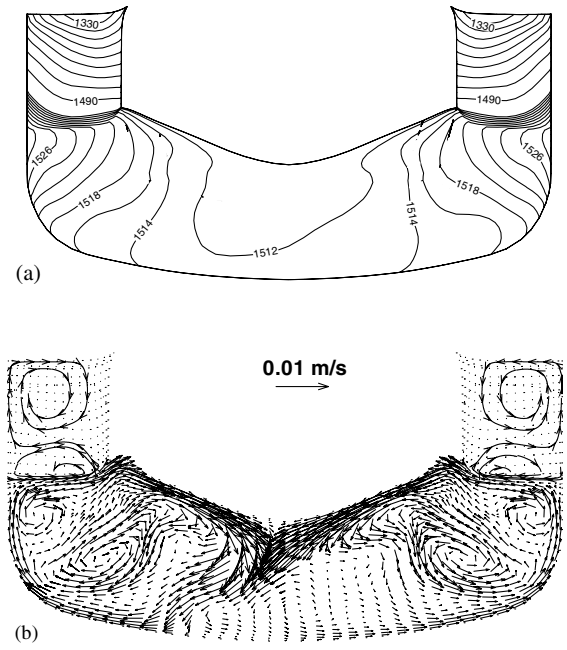

Fig. 6. Instantaneous distributions of the temperature (a) and velocity (b) in the melt and encapsulant.

the high Prandtl number of the encapsulant (see Table 1).

Of special interest is to compare the results obtained using 3D unsteady LES and results obtained using a steady RANS approach. Such a comparison is only possible for time-averaged quantities, as it is made for the time-averaged melt velocity in our paper (see Fig. 7). The presented RANS results are obtained using the low Reynolds number turbulence model of Chien [14]. One can conclude that the averaged velocity distributions differ significantly from each other. The flow structure obtained using the RANS approach consists of three toroidal vortices and the maximal velocities are lower than in the LES case. So, it is evident now that the prediction of turbulent characteristics during GaAs LEC crystal growth is of high importance because of their strong effect on the averaged melt flow structure and, consequently, due to their impact on a heat regime during the crystallization. Really, distributions of the effective viscosities referred to the melt molecular viscosity calculated for both LES and RANS cases (see Fig. 8) differ noticeably from each other. Analyzing the data obtained with LES, the following drawbacks of the RANS approach seem to be remarkable. First, the turbulent viscosity is overestimated in the melt periphery because 3D unsteady modeling predicts only slow melt pulsations there. Secondly, the RANS approach does not reproduce the active turbulent mixing in the under crystal region, revealed by LES.

Of great interest with respect to engineering applications is the prediction of the crystallization front geometry during crystal growth from a melt (see, for example, [2]). The geometry of the crystallization front determines to a large extent the crystal lattice properties

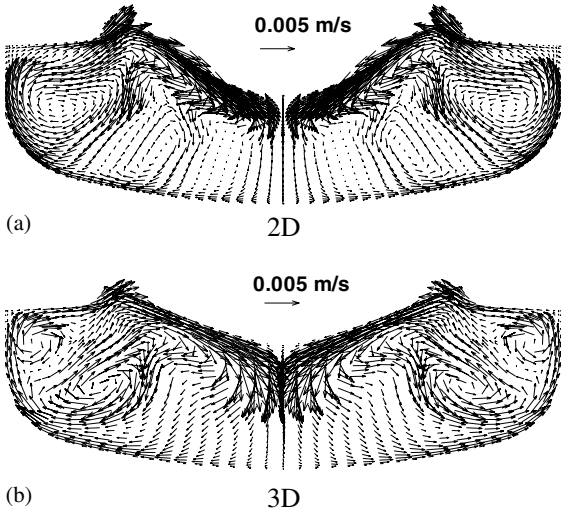

Fig. 7. The time-averaged melt velocity obtained in the RANS computation (a) and obtained in the LES computation (b).

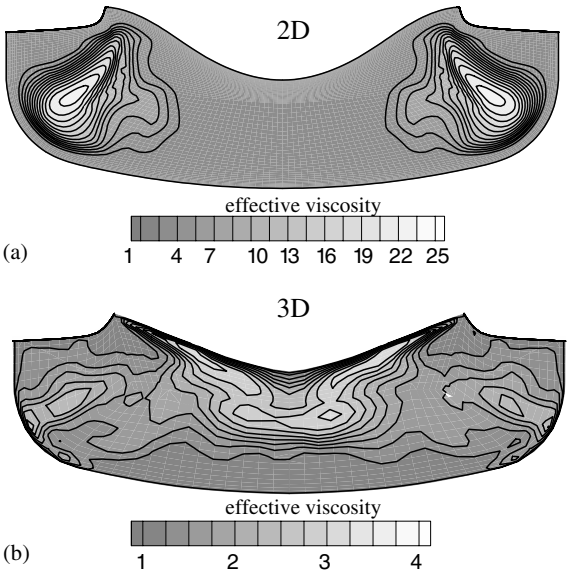

Fig. 8. The distributions of the effective viscosities referred to the melt molecular viscosity, calculated for RANS case (a) and calculated for LES case (b).

which should be precisely controlled for further successful device production [1]. We have computed the melt/crystal interface shapes for both LES and RANS cases. Fig. 9 present the deflections of the interface from the triple melt/crystal/encapsulant point. To estimate the effect of the encapsulant convection on the interface geometry, an additional calculation in terms of the 3D unsteady LES approach was carried out without the account of convective heat transport in the encapsulant, and the result is also presented in Fig. 9. It is evident that the interface predicted using the steady RANS approach is about 30% more concave into the melt than the result obtained in terms of LES. Also, there is a noticeable difference near the triple point, which is critical for the prediction of crystal surface defects [1,3]. In

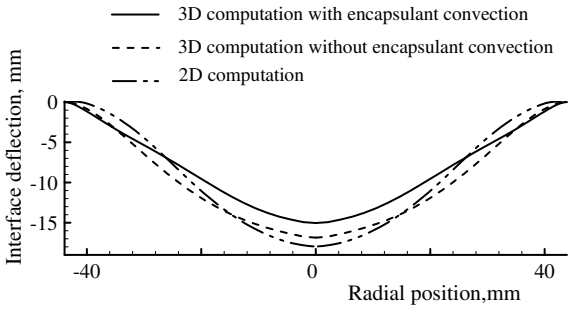

Fig. 9. Deflections of the interface from the triple melt/crystal/encapsulant point obtained in the RANS case and in LES with and without encapsulant convection.

engineering calculations [4–9], the flow of encapsulant is often ignored. However, our 3D unsteady analysis clearly indicates that the contribution of encapsulant convection into the heat exchange near the triple point is sufficiently important, comparing to the effect of melt convection. Really, ignoring the encapsulant convection can lead to the interface deflection changes of the same order as the difference between the results obtained with the RANS and LES approaches.

5. Conclusions

Test calculations in a model setup have been performed to study the interaction between turbulent and laminar flows having an immiscible interface for dimensionless parameters close to LEC GaAs growth. The testing calculations have shown that a laminar flow can affect a turbulent flow similar to a solid wall; so, the turbulent kinetic energy tends to vanish at the interface between two liquids. However, the motion of the laminar fluid may usually reflect the average direction of low frequency turbulent pulsations. In other words, the laminar flow suppresses turbulent fluctuations of high frequency and coexists with slow reconstructions of the turbulent flow.

Using the developed 3D conjugated model of heat transport and flows in the near-melt zone including the crystal, the melt, the encapsulant, and the crucibles, we have investigated details of heat and mass transfer during industrial-scale LEC growth of GaAs crystals. It was found that the flow of the GaAs melt is 3D and unsteady with turbulent regime under the crystallization front and transitional regime in the melt periphery. Using the 3D unsteady model the effect of the encapsulant flow on the formation of the crystallization front was found to be significant mainly due to the comparatively high Prandtl number of the encapsulant. In this case, even slow encapsulant motion produced by the tension from the melt flow and by the buoyancy force is sufficient to affect the melt/crystal interface geometry. Comparing the results obtained with the 3D unsteady model to results obtained with the conventional steady-state RANS approach has revealed that the prediction of turbulent characteristics is of high importance for LEC growth because of a significant effect on crystallization conditions. For example, the difference in predicting the deflection of the crystallization front if using the two approaches for turbulence simulation was found to be about 30%.

Considering the results obtained using 3D unsteady modeling, future improvement of computational models for crystal growth from the melt seems to be associated with an application of more refined numerical approximations for convective terms or with using more detailed computational grids. Also, it looks quite reliable if the DNS approach resolving well all turbulence scales will be applied soon to obtain comprehensive information about turbulent characteristics. Obtaining detailed information about turbulent heat and mass transfer during crystal growth will be used, in due course, for the calibration of conventional turbulence models used in day-to-day engineering calculations in terms of the RANS approach.

Acknowledgements

We would like to thank E.V. Yakovlev, E.M. Smirnov, and Yu.N. Makarov for fruitful discussions and for help with computations. The authors acknowledge *Istitut für Kristallzüchtung*, *Berlin*, *Germany* for support of the research.

References

[1] P. Rudolph, M. Jurisch, Bulk growth of GaAs: an overview, J. Cryst. Growth 198–199 (1999) 325–335.
[2] Ch. Frank, K. Jacob, M. Neubert, P. Rudolph, J. Fainberg, G. Müller, Temperature field simulation and correlation to the structural quality of semi-insulating GaAs crystals grown by the vapour pressure controlled Czochralsri method (VCz), J. Cryst. Growth 213 (2000) 10–18.
[3] K.K. Böttcher, P. Rudolph, M. Neubert, M. Kurz, A. Rusztai, Global temperature field simulation of the vapour pressure controlled Czochralski (VCZ) growth of 3″–4″ gallium arsenide crystals, J. Cryst. Growth 198–199 (1999) 349–354.
[4] J. Fainberg, H.-J. Leister, G. Müller, Numerical simulation of the LEC-growth of GaAs crystals with account of high-pressure gas convection, J. Cryst. Growth 180 (1997) 517–523.
[5] Y.F. Zou, H. Zhang, V. Prasad, Dynamics of melt–crystal interface and coupled convection-stress predictions for Czochralski crystal growth processes, J. Cryst. Growth 166 (1996) 476–482.
[6] J.L. Santailler, T. Duffar, F. Theodore, P. Boiton, C. Barat, B. Angelier, N. Giacometti, P. Dusserre, J.P. Nabot, Some of two commercial softwares for the modeling of bulk crystal growth processes, J. Cryst. Growth 180 (1997) 698–710.
[7] A. Seidl, S. Eicher, T. Flade, M. Jurisch, A. Köhler, U. Kretzer, B. Weinert, 200 mm GaAs crystal growth by the temperature gradient controlled LEC method, J. Cryst. Growth 225 (2001) 561–565.
[8] W. Miller, W. Schröder, Numerical modeling at the IKZ: an overview and outlook, J. Cryst. Growth 230 (2001) 1–9.
[9] W. Miller, U. Rehse, K. Böttcher, Influence of melt convection on the interface during Czochralski crystal growth, Solid-State Electron. 44 (2000) 825–830.
[10] V.I. Polezhaev, O.A. Bessonov, N.V. Nikitin, S.A. Nikitin, Convective interaction and instabilities in GaAs Czochralski model, J. Cryst. Growth 230 (2001) 40–47.

[11] K. Koai, A. Seidl, H.-J. Leister, G. Müller, A. Köhler, Modeling of thermal fluid in the liquid encapsulated Czochralski process and comparison with experiment, J. Cryst. Growth 137 (1994) 41–47.
[12] P.R. Spalart, Strategies for turbulence modeling and simulations, Int. J. Heat Fluid Flow 21 (2000) 252–263.
[13] N.G. Ivanov, A.B. Korsakov, E.M. Smirnov, K.V. Khodosevitch, V.V. Kalaev, Yu.N. Makarov, E. Dornberger, J. Virbulis, W. von Ammon, Analysis of magnetic field effect on 3D melt flow in CZ Si growth, J. Cryst. Growth 250 (1–2) (2003) 183–188.
[14] K.-Y. Chien, Predictions of channel and boundary-layer flows with low-Reynolds-number turbulence model, AIAA J. 20 (1982) 33–38.
[15] V.V. Kalaev, I.Yu. Evstratov, Yu.N. Makarov, Gas flow effect on global heat transport and melt convection in Czochralski silicon growth, J. Cryst. Growth 249 (1–2) (2003) 87–99.
[16] E.V. Yakovlev, V.V. Kalaev, I.Y.u. Evstratov, Ch. Frank-Rotsch, M. Neubert, P. Rudolph, Yu.N. Makarov, Global heat and mass transfer in vapor pressure controlled Czochralski growth of GaAs crystals, J. Cryst. Growth 252 (1–3) (2003) 26–36.
[17] T. Takeshita, T. Segawa, J.A. Glazer, M. Sano, Thermal turbulence in mercury, Phys. Rev. Lett. 76 (1996) 1465–1468.
[18] S. Cioni, S. Ciliberto, J. Sommeria, Strongly turbulent Rayleigh–Benard convection in mercury: comparison with result, J. Fluid Mech. 335 (1997) 111–140.
[19] R. Verzicco, R. Camussi, Transitional regime of low-Prandtl thermal convection in cylindrical cell, Phys. Fluids 9 (5) (1997) 1287–1295.